Dual Coenzyme Specificity of Photosynthetic Glyceraldehyde-3-phosphate Dehydrogenase Interpreted by the Crystal Structure of A 4 Isoform Complexed with NAD † , ‡

ARTICLE *in* BIOCHEMISTRY · MAY 2003

Impact Factor: 3.02 · DOI: 10.1021/bi0272149 · Source: PubMed

7 AUTHORS, INCLUDING:

Simona Fermani
University of Bologna
79 PUBLICATIONS **1,315** CITATIONS
SEE PROFILE

Francesca Sparla
University of Bologna
53 PUBLICATIONS **1,124** CITATIONS
SEE PROFILE

Paolo Trost
University of Bologna
79 PUBLICATIONS **1,953** CITATIONS
SEE PROFILE

Dual Coenzyme Specificity of Photosynthetic Glyceraldehyde-3-phosphate Dehydrogenase Interpreted by the Crystal Structure of A_4 Isoform Complexed with NAD[†,‡]

Giuseppe Falini,[§] Simona Fermani,*[,§] Alberto Ripamonti,[§] Piera Sabatino,[§] Francesca Sparla,[||] Paolo Pupillo,[||] and Paolo Trost[||]

Dipartimento di Chimica "G. Ciamician", via Selmi 2, and Laboratorio di Fisiologia Vegetale, Dipartimento di Biologia evoluzionistica sperimentale, via Irnerio 42, Alma Mater Studiorum Università di Bologna, 40126 Bologna, Italia

Received November 20, 2002; Revised Manuscript Received February 3, 2003

ABSTRACT: Photosynthetic glyceraldehyde-3-phosphate dehydrogenase (GAPDH) of *Spinacia oleracea* belongs to a wide group of GAPDHs found in most organisms displaying oxygenic photosynthesis, including cyanobacteria, green and red algae, and higher plants. As a major catalytic difference with respect to glycolytic GAPDH, photosynthetic GAPDH exhibits dual cofactor specificity toward pyridine nucleotides with a preference for NADP(H). Here we report the crystal structure of NAD-complexed recombinant A_4-GAPDH (NAD-A_4-GAPDH) from *Spinacia oleracea*, expressed in *Escherichia coli*. Its superimposition onto native A_4-GAPDH complexed with NADP (NADP-A_4-GAPDH) pinpoints specific conformational changes resulting from cofactor replacement. In photosynthetic NAD-A_4-GAPDH, the side chain of Asp32 is oriented toward the coenzyme to interact with the adenine ribose diol, similar to glycolytic GAPDHs (NAD-specific). On the contrary, in NADP-A_4-GAPDH Asp32 moves away to accommodate the additional 2′-phosphate group of the coenzyme and to minimize electrostatic repulsion. Asp32 rotation is allowed by the presence of the small residue Ala40, conserved in most photosynthetic GAPDHs, replacing bulky amino acid side chains in glycolytic GAPDHs. While in NADP-A_4-GAPDH two amino acids, Thr33 and Ser188, are involved in hydrogen bonds with the 2′-phosphate group of NADP, in the NAD-complexed enzyme these interactions are lacking. The crystallographic structure of NAD-A_4-GAPDH highlights that four residues, Thr33, Ala40, Ser188, and Ala187 (Leu, Leu, Pro, and Leu respectively, in glycolytic *Bacillus stearothermophilus* GAPDH sequence) are of primary importance for the dual cofactor specificity of photosynthetic GAPDH. These modifications seem to trace the minimum evolutionary route for a primitive NAD-specific GAPDH to be converted into the NADP-preferring enzyme of oxygenic photosynthetic organisms.

Plants possess four different genes for phosphorylating glyceraldehyde-3-phosphate dehydrogenases (GAPDH)[1]. GapA and GapB code for precursors of GAPDH subunits A and B, which contain a transit peptide for plastids. The processed subunits are assembled into two different isoforms of this photosynthetic enzyme, having either A_4 or A_nB_n stoichiometry (EC 1.2.1.13) (*1*, *2*). The minor A_4 variant has been defined nonregulatory (*3*), as opposed to the major regulatory (A_nB_n) isoform. The association behavior and activity of this AB isoform are affected by thioredoxins and hysteretically modulated by substrates, chiefly NAD(P) and 1,3-bisphosphoglycerate (*4*−*9*). A third plant gene (GapC) encodes a NAD-specific GAPDH involved in cytosolic glycolysis (EC 1.2.1.12), a really ubiquitous enzyme of bacteria and eukaryotes (*10*). Finally, a GapCp gene has been described for a few plant species as a plastid-located counterpart of cytosolic GapC (*11*).

Chloroplast GAPDH catalyzes a unique step of the photosynthetic carbon reduction cycle. Both A_4 and AB isoforms are able to use either NADP(H) or NAD(H) as coenzymes, although the NADP-dependent catalysis is more efficient than the NAD-dependent one (*3*, *12*). Consistent with the endosymbiotic origin of chloroplasts, GapA and GapB genes of higher plants and most eukaryotic photosynthetic organisms are closely related to Gap2 of cyanobacteria, which is also active with both NADP and NAD (*13*). All these plant GAPDH genes are related to, and probably derived from, an early prokaryotic gene similar to GapC (and likewise NAD-specific) (*14*). The kinetic preference for NADP over NAD in photosynthetic GAPDHs is understood as an adaptation to the reducing pyridine nucleotide prevailing in oxygenic photosynthesis (i.e., NADPH).

[†] Financial support from the Ministero dell'Università e della Ricerca Scientifica and the University of Bologna (funds for selected research topics) is gratefully acknowledged.

[‡] Protein coordinates have been deposited in the Protein Data Bank (PDB ID 1NBO).

* Corresponding author. Phone: +39-051-2099484. Fax: +39-051-2099456. E-mail: fermani@ciam.unibo.it.

[§] Dipartimento di Chimica "G. Ciamician".

[||] Laboratorio di Fisiologia Vegetale, Dipartimento di Biologia evoluzionistica sperimentale.

[1] Abbreviations: NAD-A_4-GAPDH, spinach chloroplasts glyceraldehyde-3-phosphate dehydrogenase (recombinant form) complexed with NAD; NADP-A_4-GAPDH, as above but native and purified from chloroplasts, complexed with NADP; *B. st.*, *Bacillus stearothermophilus*; rmsd, root-mean-square deviation.

10.1021/bi0272149 CCC: $25.00
Published on Web 04/01/2003

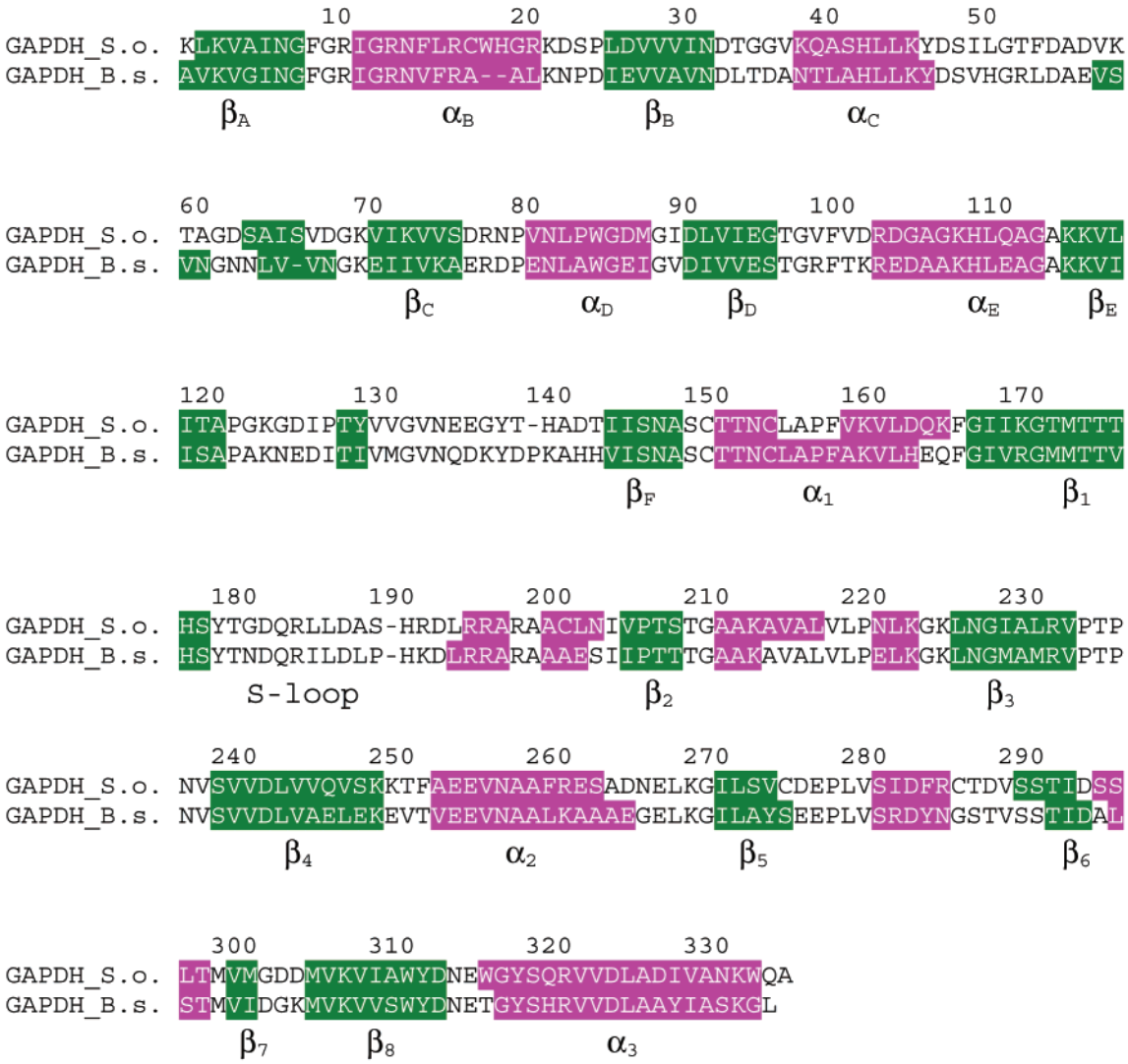

FIGURE 1: Sequence and secondary structure alignment of subunit A of chloroplast GAPDH from *Spinacia oleracea* and of cytosolic GAPDH from *Bacillus stearothermophilus*. The α-helix portions of the sequence are indicated in magenta, *β*-strand in green. Abbreviations: S.o., *Spinacia oleracea*, B.s. *Bacillus stearothermophilus*.

Cytosolic, NAD-dependent GAPDH is a well-known enzyme, and many tridimensional structures from different organisms have been solved (*15*−*27*), all showing a common organization. The monomers, each consisting of two folding domains, associate into tetramers with a noncrystallographic 222 symmetry. The coenzyme (NAD) is present in an extended conformation and set in place by several hydrogen bonds and hydrophobic interactions. In particular, the carboxylate group of Asp32 chelates the 2′,3′-diol of the adenine ribose. Coenzyme specificity in most NAD-dependent oxidoreductases is primarily ascribed to analogous interactions between an Asp (rarely Glu) side chain and the adenine ribose diol (*28*). In NADP-dependent oxidoreductases, on the other hand, the additional 2′-phosphate of the coenzyme is usually engaged in a salt bridge with the positive side chain of an arginine (rarely Lys) (*28*).

We have recently reported the first crystallographic structure of a photosynthetic GAPDH (the nonregulatory A_4 isoform of spinach chloroplasts), complexed with NADP (*29*). The basic features of this structure are closely related to known glycolytic GAPDHs. Despite the remarkable catalytic preference of photosynthetic GAPDH for NADP over NAD (*3*, *12*), Asp32 is fully conserved (Figure 1) (*30*), and the binding of NADP is made possible by the rotation of Asp32, thus avoiding any repulsion with the 2′-phosphate of the coenzyme. Moreover, NADP-binding is facilitated by residues Thr33 and Ser188, the latter belonging to a symmetry related monomer, which stabilize the 2′-phosphate of NADP by hydrogen bonds. Here we report the crystal structure of NAD-complexed recombinant A_4-GAPDH from *Spinacia oleracea*, expressed in *Escherichia coli*. A comparison of the two complexes provides a molecular interpretation of the dual cofactor specificity of this dehydrogenase, based on specific and significant changes of the tridimensional structure.

MATERIALS AND METHODS

Expression, Purification, and Enzyme Activity. Recombinant expression and purification of A_4-GAPDH from *S. oleracea* has been performed as described by Sparla et al. (*9*). Protein solutions for crystallization contained pure protein at 10 mg mL^{-1} in 25 mM Tris-HCl (pH 7.5) and 1 mM NAD.

Standard enzyme activity was performed at 298 K in 50 mM Tris-HCl, 1 mM EDTA, 5 mM $MgCl_2$, 3 mM 3-phos-

Table 1: Unit Cell Parameters and Data Collection Statistics

space group	C222
unit cell (Å)	$a = 140.6$, $b = 185.6$, $c = 106.4$
resolution limits (Å)	90−2.6
measured reflections	679 015
unique reflections	43 271
R_{sym} (%)	9 (20)[a]
completeness (%)	99.9 (99.9)[a]
I/σ (I)	26 (9)[a]
redundancy	8.5

[a] The values in parentheses refer to the last resolution shell from 2.69 to 2.6 Å.

phoglycerate, 2 mM ATP, 5 U mL^{-1} phosphoglycerate kinase (from rabbit muscle), and 0.2 mM NADPH. Oxidation of NADPH was followed at 340 nm with an ϵ_{340} of 6.23 mM^{-1}. For steady-state kinetic analysis, activities were measured at variable concentrations of NAD(P)H (5−300 μM) and 3-phosphoglycerate (0.2−4 mM). The equilibrium concentration of the substrate 1,3-bisphosphoglycerate was calculated on the basis of the K_{eq} for phosphoglycerate kinase of 3.1×10^{-4} (*31*). Activity data points were fit by nonlinear regression analysis (CoStat, CoHort Software) to the equation of a Ping Pong reaction mechanism (*32*):

$$v = (V_{max}AB)/(K_{m(B)}A + K_{m(A)}B + AB)$$

where A and B are the concentrations of NAD(P)H and 1,3-bisphosphoglycerate, respectively.

Crystallization and Data Collection. Crystals of A_4-GAPDH complexed with NAD were grown at 293 K using the hanging drop vapor diffusion technique. The 4 μL droplets formed by the protein solution and the reservoir were equilibrated over wells containing 0.750 mL of 1 M $(NH_4)_2SO_4$ and 0.1 M Tris-HCl (pH 8). For data collection at 100 K, the crystals were transferred in different solutions containing 1.8 M $(NH_4)_2SO_4$, 1 mM NAD, and glycerol as a cryoprotectant, starting from a glycerol concentration of 10% (v/v) to a final concentration of 40% (v/v). The diffraction data, with a resolution limit of 2.6 Å, were collected at the Elettra X-ray diffraction beam line (Trieste, Italy). They were processed and scaled using DENZO and SCALEPACK programs (*33*). The crystals belong to the space group C222, and they are isomorphous with those of the native A_4-GAPDH complexed with NADP (*34*). The unit cell parameters and the data collection statistics are shown in Table 1.

Structure Solution and Refinement. The NAD-A_4-GAPDH structure was solved by the molecular replacement method with the program AMoRe (*35*) using the native chloroplast A_4-GAPDH model (*29*) (Protein Data Bank access number 1JN0) without cofactor, sulfate ions, and water molecules. Similar to the native structure, the asymmetric unit contains three subunits named O, O′, and R′.

The refinement was carried out in a resolution range of 8.0−2.6 Å using CNS (*36*). The model building was performed with the graphic program O (*37*). A total of 5% of the data were randomly selected for R_{free} calculations. Noncrystallographic symmetry (NCS) restraints with different weights on main chain and side chain atoms were applied during the initial runs of refinement. After the model was refined to an R_{factor} of 27.8%, the electron density map revealed unambiguously the position of NAD in all the three monomers. Additionally, two sulfate ions for each monomer were built into the active site according to the electron density map. At an R_{factor} value of 26%, the NCS restraints were removed.

Table 2: Steady-State Kinetic Parameters of Recombinant A_4-GAPDH from Spinach Chloroplasts

		Coenzyme	
kinetic parameter	unit	NADPH	NADH
k_{cat}	s^{-1}	61 ± 4	41 ± 9
$K_{m(coenzyme)}$	μM	29 ± 8	140 ± 38
$K_{m(BPGA*)}$[a]	μM	13 ± 2	12 ± 3
k_{cat}/K_m	$s^{-1}\,M^{-1}$	2.1×10^6	2.9×10^5

[a] *BPGA: 1,3-bisphosphoglycerate.

The R_{factor} and R_{free} dropped down to the final values of 20.3% (23.2% in the highest resolution bin corresponding to 2.76−2.60 Å) and 24.5% (28.8% in the highest resolution bin), respectively, after introducing water molecules. They were positioned only where the stereochemistry and the interactions were favorable and both the $(2F_o - F_c)$ and the $(F_o - F_c)$ difference Fourier maps showed a density of more than 0.8σ and 3.0σ, respectively. Two sulfate ions (indicated as C1 and C2, respectively) were also positioned with the same criteria applied to the water molecules at the surface of monomers R′ and O′, respectively.

The average thermal parameter (B) for the whole model is 34.9 Å^2, while the average B values are 21.2, 37.8, and 45.1 Å^2 for the protein chains O, O′, and R′, respectively, 20.6, 44.2, and 49.7 Å^2 for NAD atoms belonging to monomer O, O′, and R′, respectively, 48.2 Å^2 for sulfate ions found in monomer O (refined with an occupancy value of 1.00), 58.8 and 55.5 Å^2 for sulfate ions found in monomers O′ and R′, respectively (refined with an occupancy value of 0.75), 61.8 Å^2 for sulfate ion C1, and 65.8 Å^2 for sulfate ion C2 (refined with occupancy values of 1.00 and 0.50, respectively). The 359 water molecules show an average B value of 31.1 Å^2 (for the 189, 101, and 69 water molecules in monomers O, O′, and R′, respectively, the B values are 28.5, 34.3, and 31.2 Å^2).

RESULTS

Kinetic Characterization of Recombinant A_4-GAPDH. The subunit A of spinach photosynthetic GAPDH was heterologously expressed in *E. coli* and purified to homogeneity as a homotetramer, A_4 (*9*). Steady-state kinetic analysis of purified recombinant A_4-GAPDH (Table 2) revealed similar kinetic parameters to native A_4-GAPDH purified from spinach chloroplasts (*3*). In particular, the NADPH-dependent reaction was confirmed to be kinetically more efficient than the NADH-dependent reaction. With respect to NADH, the k_{cat} with NADPH was higher by a factor of 1.5, and the $K_{m(NADPH)}$ was lower by a factor of 4.7. As a result, the specificity constant k_{cat}/K_m for NADPH was 7-fold higher than for NADH. On the other hand, affinity for the substrate 1,3-bisphosphoglycerate did not depend on the type of coenzyme used as an electron donor (Table 2).

Crystal Structure of NAD-A_4-GAPDH. In analogy with native chloroplast A_4-GAPDH complexed with NADP (*29*), the final model of the recombinant form complexed with NAD is made up of three monomers in the asymmetric unit of the C222 space group. The monomers indicated as O, O′,

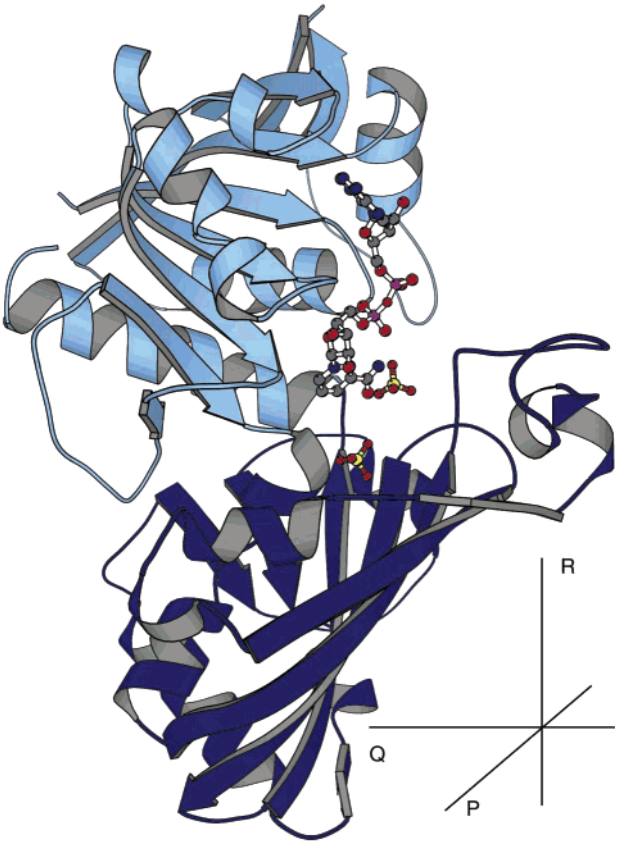

FIGURE 2: Overall fold of the monomer of recombinant chloroplast GAPDH complexed with NAD. The cofactor-binding and catalytic domains are in light and dark blue, respectively. The figure was produced using the program MOLSCRIPT (*51*).

and R′ have been named according to *B. st.* (*38*) and native chloroplast A_4-GAPDH models (*29*), and the residues have been numbered to maximize the homology between the sequences. Monomers O and O′ contain residues 1−334, whereas monomer R′ contains residues 1−333 because of the lack of electron density corresponding to the C-terminal residue Ala334. Residues Arg22 and Asp67, absent in the model of the native structure (*29*), were correctly positioned in the recombinant structure.

The crystal packing of NAD-A_4-GAPDH is the same as in the native form (*29*). The position of the monomer O is close to the cell origin, and the crystallographic equivalents P, Q, and R are created by the 222 symmetry operation. Thus, the three molecular axes of the tetramer (P axis between O and P subunits, R axis between O and R subunits, and Q axis between O and Q subunits) correspond to the crystallographic ones (Figure 2). A second tetramer with a pseudo-222 symmetry is formed by the dimer O′R′ using a crystallographic 2-fold axis coincident with the molecular axis P. Although noncrystallographic symmetry restraints were not employed in the final cycles of the refinement process, the conformations of subunits O, O′, and R′ in the final model are quite similar. The superimposition of the backbone atoms of the O subunit, used as a reference, and O′ and R′ subunits gave root-mean-square deviations of 0.290 and 0.303 Å, respectively. The rmsd resulting from the backbone atoms superimposition of O′ and R′ subunits was 0.341 Å.

Each monomer comprises one NAD molecule, characterized by a well-defined electron density in all three subunits. The NAD is bound to the protein in an extended conformation as previously observed for *B. st.* GAPDH, kept in place by several hydrogen bonds (Table 3). The adenine and nicotinamide rings are roughly perpendicular to the average planes of the neighboring riboses. The conformation of the adenine is anti and that of the nicotinamide ring is syn. The planar adenine is located between the methyl groups of two threonine residues (33 and 96). The orientation of the nicotinamide ring is stabilized by an intramolecular hydrogen bond, involving the NAD atoms NO1 and NN7, and by a hydrophobic interaction with the side chain of Ile11, while a different orientation is sterically hindered by the Tyr311 side chain. Both furanose rings are in C2′-*endo* conformation.

Table 3: Interactions Involving NAD Molecule

A. Shortest contacts (less than 3.5 Å) with protein atoms and sulfate ion

		Distance (Å)		
		O	O′	R′
NAD-AN6	Arg77-O	3.09	3.06	3.16
NAD-AO2*	Asp32-OD1	3.21	2.98	3.29
NAD-AO3*	Asp32-OD2	2.69	2.67	3.13
NAD-AO3*	Gly9-N	3.36	3.41	>3.50
NAD-AO2	Arg10-N	3.02	2.99	2.94
NAD-NO2	Ile11-N	2.90	2.89	2.97
NAD-NO2*	$SO_4$338-O	3.15	3.38	2.87
NAD-NO4*	Thr119-OG1	3.45	3.44	3.45
NAD-NO7	Asn313-ND2	2.88	>3.50	2.80

B. Shortest contact (less than 3.5 Å) with solvent molecules

	O	distance (Å)	O′	distance (Å)	R′	distance (Å)
NAD-AO1	W222	2.70	W351	3.08		
NAD-AO2	W231	3.16				
NAD-AO2	W236	2.74	W258	2.79		
NAD-AO3*	W263	2.82				
NAD-O3	W222	3.11				
NAD-NO1	W6	2.78	W259	2.92		
NAD-NO1	W176	2.60				
NAD-NO2	W73	3.05	W190	2.69		
NAD-NO2*	W140	2.61	W246	2.76		
NAD-NO3*	W35	3.01	W174	3.12		
NAD-NO3*	W15	3.02	W188	3.19	W298	2.85

In analogy with cytosolic GAPDHs, two sulfate ions from the crystallization medium are positioned in the active site of each subunit. These anion sites were suggested to correspond, respectively, to the positions of the $C_{(3)}$ phosphate of the substrate (site P_s) and of the inorganic phosphate ion (site P_i) responsible for the phosphorylation step during catalysis (*39*). However, an alternative model predicts that the $C_{(3)}$ phosphate of the substrate (glyceraldehyde-3-phosphate) first occupies the P_i site and successively flips to the P_s site, thus making the P_i site available for the inorganic phosphate (*18*, *40*).

The electron density map clearly shows two additional sulfate ions located on the surface of subunits O′ and R′. The sulfate ion C1 is stabilized by a network of hydrogen bonds with water molecules (W295 and W127) and with the main chain atoms Gly252 N and Val299 O belonging to subunit R′ and by an electrostatic interaction with Lys72 of subunit O. The sulfate ion C2 is kept in place by the positive residue Arg80 of subunit O′. In addition, the asymmetric unit contains 359 water molecules.

Model Quality. The final model has tight stereochemical restraints with root-mean-square deviations from ideal values on bond lengths of 0.006 Å and on bond angles of 1.3°. The

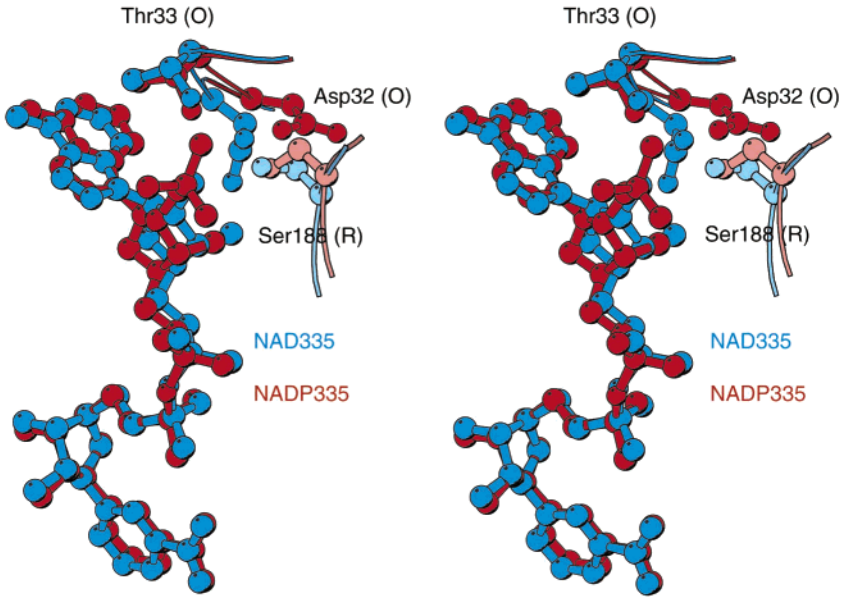

FIGURE 3: Stereoview of the superimposition of the cofactor-binding site of recombinant chloroplast A_4-GAPDH complexed with NAD (blue; R-related subunit in light blue) and of native chloroplast A_4-GAPDH complexed with NADP (red; R-related subunit in salmon). The figure was produced using the program MOLSCRIPT (*51*).

majority of residues lie in the most favored regions of the Ramachandran plot as defined by PROCHECK (*41*). Only Val237 and Trp332 are in disallowed regions. The unfavorable dihedral angles of the conserved residue Val237 (Figure 1), which shows a well-defined electron density, have been already observed in NADP-A_4-GAPDH (*29*) and most cytosolic GAPDH structures (*18*, *22*, *24*). To estimate the root-mean-square error in the atomic positions, the Luzzati method was applied (*42*). The plot (not shown) gave an estimated value of 0.28 Å for the overall mean positional error.

Comparison between Photosynthetic NAD-A_4-GAPDH and NADP-A_4-GAPDH. The superimposition of monomer O of recombinant GAPDH complexed with NAD and native GAPDH complexed with NADP (*29*) (rmsd value for 320 C_α atoms of 0.383 Å) pinpoints a few but significant conformational changes occurring when the cofactor is replaced. As found for cytosolic NAD-GAPDHs (*15*−*25*), in photosynthetic NAD-A_4-GAPDH the side chain of Asp32 is oriented toward the coenzyme to interact with the adenine ribose diol (Table 3), while in NADP-A_4-GAPDH Asp32 moves away (Figure 3) to accommodate the additional 2′-phosphate of the coenzyme and to minimize the electrostatic repulsion (*29*). The root-mean-square deviations calculated from the superimposition between NAD-A_4-GAPDH and NADP-A_4-GAPDH in residues 31−36 (Figure 1) are 0.539 Å on backbone atoms and 1.128 Å if both main chain and side chain atoms are considered.

Whereas in the NADP-complex the OH groups of Thr33 and Ser188 (the latter belonging to the S-loop of the R related subunit) are involved in hydrogen bonds with the 2′-phosphate group of NADP, the Thr33 interaction fails to occur in the NAD-complexed enzyme (Figure 3). In a similar fashion, Ser188 does not interact with the coenzyme any more and interacts with a water molecule in monomer O (Ser188 OG-W323 O 3.73 Å) and with Asn39 of the R related subunit in monomer O′ and monomer R′ (Ser188 (O′) OG-Asn39 (R′) OE1 2.95 Å and Ser188 (R′) OG-Asn39 (O′) OE1 2.67 Å).

In the catalytic domain of the NAD-A_4-GAPDH, the most significant difference with respect to NADP-A_4-GAPDH involves the sulfate ion $SO_4$339, labeled $SO_4$337 in Fermani et al. (*29*), in P_i position (*39*). This sulfate moves toward $SO_4$338, labeled $SO_4$336 in Fermani et al. (*29*), P_s site (Figure 4) by about 2.42 Å in monomer O and 1.48 Å in monomers O′ and R′. The sulfate ions have been positioned where the ($2F_o - F_c$) electron density showed its maximum. In monomer O, showing the largest $SO_4$339 displacement, a small positive ($F_o - F_c$) density is observed in a position corresponding to the P_i site of NADP-A_4-GAPDH structure, suggesting a minimal partial occupation of this location by the sulfate ion. Instead, in monomers O′ and R′, where the $SO_4$339 displacement value is lower, small positive ($F_o - F_c$) densities are found in the positions corresponding to the location of the ion in subunit O of NAD-A_4-GAPDH and to the P_i site of NADP-A_4-GAPDH. However, number and type of interactions of $SO_4$339 are not changed in the different positions. In fact, the interaction with Ser148 ($SO_4$339 (O) O2−Ser148 (O) OG 2.86 Å, $SO_4$339 (O′) O1−Ser148 (O′) OG 3.58 Å, and $SO_4$339 (R′) O2−Ser148 (R′) OG 2.99 Å) is conserved in both structures, and the proton-donor role of Thr208 in NADP-A_4-GAPDH is partially replaced in NAD-A_4-GAPDH by the conserved hydroxylated residue Thr150 ($SO_4$339 O4−Thr150 OG1 2.72, 2.53, and 2.85 Å in monomers O, O′, and R′, respectively). The $SO_4$339 is also stabilized by several hydrogen bonds with water molecules. The anion interacts with the catalytically important residues Cys149 and His176 in monomer O ($SO_4$339 O2−Cys149 SG 3.32 Å and $SO_4$339 O3−His176 NE2 3.86 Å), while in the other two subunits the distances exceed 4 Å. While the P_i position in native chloroplast NADP-A_4 is that found in most GAPDHs, including *B. st.* enzyme (*18*) (Figure 4), the P_i displacement found in NAD-A_4-GAPDH is similar to that observed in the active site of GAPDHs from *Leishmania mexicana* (*20*) and *Thermotoga maritima* (*21*), carboxymethylated GAPDH from *Palinurus versicolor* (*43*) and apo-GAPDH from *E. coli* containing the hemiacetal

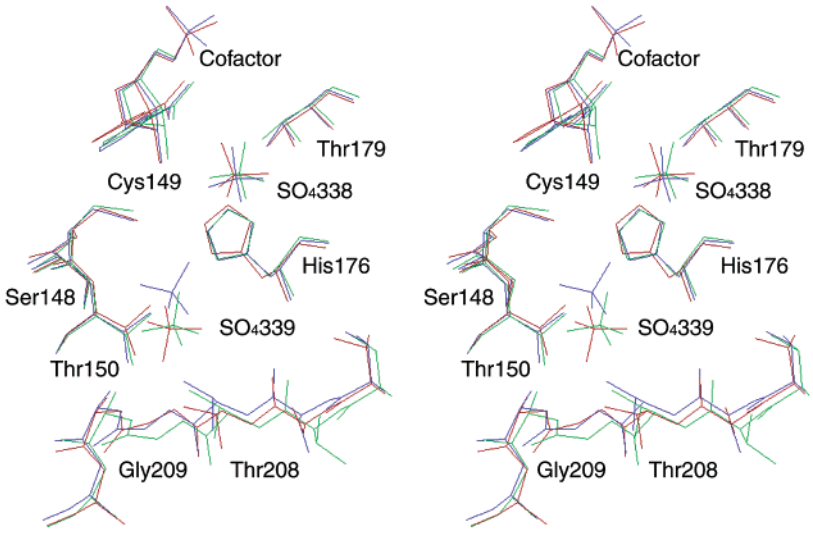

FIGURE 4: Stereoview of the superimposition of the sulfate-binding site of recombinant chloroplast A_4-GAPDH complexed with NAD (blue), native chloroplast A_4-GAPDH complexed with NADP (red), and cytosolic GAPDH from *Bacillus stearothermophilus* (green). In monomer O of the NAD-complex the sulfate ion is located near Cys149 (SO_4 O2−Cys149 SG 3.32 Å) and His176 (SO_4 O3−His176 NE2 3.86 Å), comparable to the Cys149 SG-His176 NE2 distance (3.39 Å). The presence of two threonine residues (Thr208 and Thr150), located at two different edges of the cavity, ensures that number and type of interactions formed by the $SO_4$339 are the same in different locations. The figure was produced by the program MOLSCRIPT (*51*).

intermediate of GAP bound to the active site (*44*). In these structures, the positioning of the anion (phosphate or sulfate) in the so-called "new P_i" site (as opposed to the "classical P_i" site conserved in almost all GAPDH structures) is necessary to accommodate a different conformation of the region involving residues 206−211 (corresponding to 224−229 in GAPDH from *L. mexicana*). This region shows a strand−loop−helix structure, and its peculiar conformation is not observed in NAD-A_4-GAPDH that superimpose to NADP-A_4- and *B. st.* GAPDHs with root-mean-square deviations (calculated for the backbone atoms in residues 203−214) of 0.222 and 0.168 Å, respectively. Large conformational differences result instead from the superimposition of NAD-A_4- with *L. mexicana* GAPDHs in the residue segment 203−214 (221−232 for *L. mexicana*; rmsd 1.060 Å for backbone atoms).

Ion $SO_4$338 (P_s site) shows a well-defined electron density and occupies the same position in both NAD and NADP complexes (Figure 4). This sulfate ion is stabilized, on one hand, by hydrogen bonds with the conserved Thr179 (averaged distance $SO_4$338 O−Thr179 OG1 for the three subunits 2.69 Å), and on the other hand, by electrostatic interactions with the two conserved residues Arg231 and Arg195 and with the positive charged cofactor. It is also hydrogen-bonded to the 2′-hydroxyl of the nicotinamide ribose of NAD (Table 3).

Two disulfide bridges connecting the Cys200 of monomers O and R (similarly O′ and R′) and P and Q (similarly P′ and Q′), respectively, were observed in the tetramer of native NADP-A_4-GAPDH (*29*). In recombinant NAD-A_4-GAPDH, Cys200 partly switches to a different conformation, with similar distances of the disulfide bridge. In monomer O, most molecules adopt a conformation (Cys200(O) SG−Cys200 (R) SG 2.51 Å) for which the occupancy of Cys200 sulfur atom SG has been refined to 0.70. For dimer O′R′ the distance between Cys200(O′) SG and Cys200(R′) SG corresponds to 2.04 Å.

Comparison between Photosynthetic NAD-A_4-GAPDH and Cytosolic Bacillus stearothermophilus GAPDH. The least-squares superimposition of chloroplast NAD-GAPDH and *B. st.* GAPDH O monomers shows a rmsd value of 0.670 Å for 317 superimposed C_α atoms. The conformation of the coenzyme is very similar (Figure 5), and the superimposition of the protein region interacting with the adenine moiety of NAD is quite good. Number and type of interactions between cofactor and enzyme are also similar. Only the hydrogen bond that connects the side chain of Asn180 (atom ND) and the oxygen atom AO2 of NAD (Figure 5) is lost since in chloroplast GAPDH this residue is replaced by glycine (Figure 1). The distance between the carboxylate group of Asp32 and the adenine ribose diol is longer in NAD-A_4-GAPDH (Table 3) than in *B. st*. enzyme (*18*), suggesting a weaker stabilization of the cofactor in the former. Interestingly, in *B. st*. GAPDH any movement of Asp32, as seen in chloroplast GAPDH complexed with NADP, would be prevented by the prominent side chain of Leu40 (Figure 5).

As already mentioned, the most significant deviation in the catalytic domain is determined by the position of the $SO_4$339, which exactly matches the classical P_i site in *B. st*. GAPDH and in native NADP-A_4-GAPDH but occupies the "new P_i" site in NAD-A_4-GAPDH (Figure 4).

DISCUSSION

Most organisms displaying oxygenic photosynthesis, including cyanobacteria, green and red algae, and higher plants contain photosynthetic GAPDH beside glycolytic one (*14*). Major catalytic differences between these enzymes include cofactor specificity: photosynthetic GAPDHs display dual specificity toward pyridine nucleotides, while glycolytic GAPDHs are strictly NAD-specific. Photosynthetic A_4-GAPDH of *S. oleracea* is therefore active with both NADPH and NADH, although showing a kinetic preference for the former coenzyme. That chloroplast GAPDH can efficiently use NADPH as an electron donor is entirely

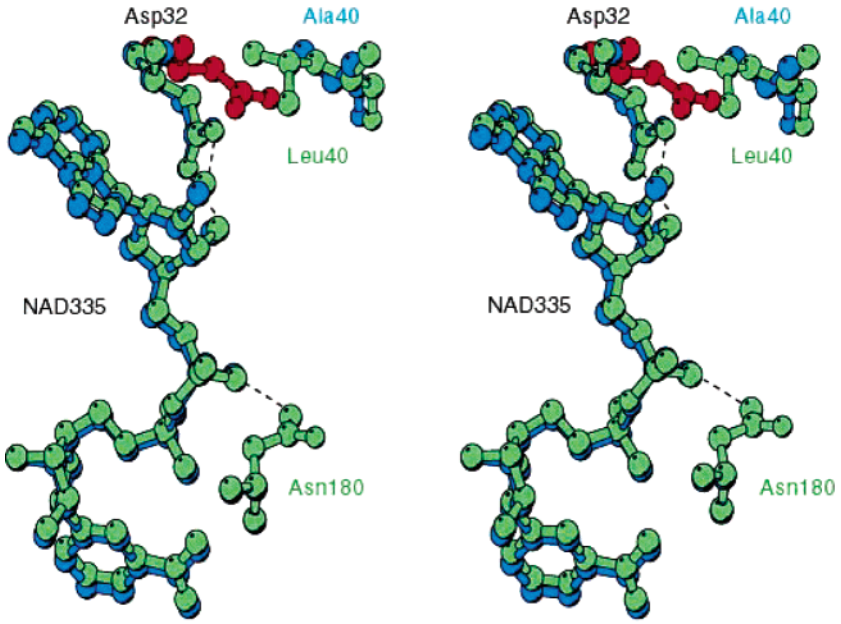

FIGURE 5: Stereoview of the superimposition of the cofactor-binding site of recombinant chloroplast A_4-GAPDH complexed with NAD (blue) and cytosolic GAPDH from *Bacillus stearothermophilus* (green). The position of the Asp32 in native A_4-GAPDH complexed with NADP is shown in red. The figure was produced by the program MOLSCRIPT (*51*).

consistent with its role in the Calvin cycle. The cycle in oxygenic phototrophs is fuelled by NADPH provided by photosystem I via ferredoxin: NADP reductase, which is an NADP-specific enzyme (*45*). Photosynthetic GAPDH is derived from an NAD-specific prokaryotic precursor (*14*), and the NAD-dependent activity of photosynthetic GAPDH might be a mere remnant of such an ancient relationship. However, photosynthetic GAPDH may also contribute to the glycolytic pathway of plastids, where the use of NAD as the dark coenzyme is probably important (*46*).

In NAD-A_4-GAPDH, the coenzyme is bound to the protein in a similar fashion as in all known GAPDHs (*15*−*25*). Comparison between the structure of NAD-A_4-GAPDH and *B. st.* GAPDH shows, for instance, that all protein−NAD interactions are conserved, except for one hydrogen bond (NAD AO2−Asn180 ND) found exclusively in the NAD-site of *B. st.* GAPDH, which, however, may play a role in enzyme stability in these thermophilic organisms (*18*).

As a distinctive feature of NAD-complexed GAPDHs, including present species, the carboxylic group of Asp32 participates in coenzyme stabilization by chelating the diol group of the adenine ribose. In the formerly described NADP-complex of chloroplast enzyme (*29*), the NADP induces a rotation of Asp32 in the opposite direction thereby minimizing the steric hindrance and electrostatic repulsion with its 2′-phosphate group. This movement is made possible by the flexibility of the short loop connecting strand β_B and helix α_C (Figure 1). In *B. st.* GAPDH, as in most glycolytic GAPDHs, Leu187 and Pro188 belonging to the S-loop fill the space corresponding to the 2′-phosphate of NADP, further contributing to the strict NAD specificity of these dehydrogenases. The less bulky Ala187 and Ser188 found in the chloroplast sequence (Figure 1) allow the positioning of NADP and stabilize it by a hydrogen bond formed between the hydroxylated residue (Ser188) and the coenzyme 2′-phosphate group. Here, we have shown that these residues do not exhibit any interaction with the coenzyme when chloroplast GAPDH is complexed with NAD.

NADP-dependent GAPDHs have been also found in few nonphotosynthetic organisms, but none of these enzymes show the same molecular determinants for coenzyme specificity as photosynthetic GAPDH. Beside the classical NAD-dependent GAPDH, in *Bacillus subtilis* an NADP-preferring GAPDH is expressed under gluconeogenic growth conditions. Even though this peculiar GAPDH shows extended sequence homologies to photosynthetic GAPDH, residue Asp32 is replaced by Ala, so that the mechanism of coenzyme selectivity is expected to be different from the spinach enzyme (*47*). Also, the fungus *Kluyveromyces lactis* contains a dual-specific GAPDH beside the classical NAD-specific isozyme, but the position 46 (corresponding to position 32 in chloroplast and cytosolic GAPDHs) is occupied by Asn instead of Asp, suggesting again a different strategy to set the preference toward pyridine nucleotides (*48*).

Clermont et al. (*49*) obtained a site-directed mutant of *B. st.* GAPDH with both Leu187 and Pro188 substituted by the corresponding residues of photosynthetic GAPDH (Ala187, Ser188) and with the Leu33−Thr34−Asp35 segment, corresponding to the important loop between β_B and α_C, replaced by the invariant photosynthetic sequence Thr33−Gly34−Gly35 (*49*). These mutations resulted in a slow NADP-dependent activity with low k_{cat} and low affinity for NADP, while the NAD-dependent activity was only slightly affected with respect to the wild-type. The superimposition of the cofactor-binding regions of NAD-A_4-GAPDH, NADP-A_4-GAPDH, and the aforementioned quintuple mutant of *B. st*. GAPDH complexed with either NAD or NADP shows a close conformation of residues Thr33−Gly35, which is quite different in wild-type *B. st.* enzyme. The reason for the failure in obtaining an efficient NADP-dependent *B. st*. GAPDH is apparently due to the bulky Leu40, which prevents the rotation of Asp32 required to accommodate the extra 2′-phosphate of NADP (Figure 5). Interestingly, the alanine residue found in the corresponding position of spinach chloroplast GAPDH is strictly conserved in all photosynthetic

GAPDH sequences of eukaryotic organisms, being replaced by Asn in NAD(P)-dependent Gap2 of most cyanobacteria (*13*, *14*).

Thermodynamic studies have shown that the higher affinity of *E. coli* dihydrodipicolinate reductase for NADH as compared to NADPH can be explained by a larger contribution of the entropic term to the binding free energy (*50*). This suggests that the increase of the entropic term because of the free aspartic residue (Asp32) in the NADP-complex can give a further contribution to coenzyme specify.

An appreciable shift of $SO_4$339 anion toward the P_s site and the catalytically important residues Cys149 and His176 has been observed in NAD-A_4-GAPDH with respect to the position of the Pi site found in native NADP-A_4 and in *B. st.* GAPDH (Figure 4). This position corresponds in monomer O to the "new P_i" site observed in several GAPDH structures reported in the literature (*20*, *21*, *43*, *44*). In these structures, the repositioning of the P_i site is accompanied by an unusual conformation of the region spanning residues Thr206−Ala211 that follow the inorganic anion forming with its oxygen atoms several hydrogen bonds. These involve the hydroxyl group of Thr208 (226 for *L. mexicana*) and the main chain N atom of Gly209 (227 for *L. mexicana*). An additional hydrogen bond between Thr150 OG (167 for *L. mexicana*) and the inorganic anion is specific of the "new P_i" site. In recombinant A_4-GAPDH complexed with NAD, the region 206−211 is conformationally very close to that in NADP-A_4-GAPDH and in *B. st.* GAPDH. As a consequence, the $SO_4$339 of NAD-A_4-GAPDH, located in the "new P_i" site, loses its hydrogen bond with Thr208, which is too far, but it gains a similar bond with Thr150. Since the different conformation in residues 206−211 cannot be ascribed to sequence variations, as previously observed (*20*, *21*,*43*, *44*), it is difficult to justify the different location of the P_i site. However, in the absence of the conformational change in residues 206−211, the cavity, which hosts SO_4-339 is large as compared to the anion size and allows some changes in the position of the latter. In fact, $SO_4$339 occupies the "classical P_i" site in native NADP-A_4, the "new P_i" site in monomer O of recombinant NAD-A_4, and intermediate positions in monomers O′ and R′ of the same structure. Spinach A_4-GAPDH is less active with NADH than with NADPH by a factor of 1.5−2.0 in terms of k_{cat} (this paper and ref *3*, respectively), and the nicotinamide moiety (the catalytically active head of the coenzyme) is exactly in the same position in both NAD- and NADP-complexes. The position occupied by $SO_4$339 is the unique notable difference between the active sites of NAD and NADP complexes. However, in consideration that in GAPDH structures crystallized up to date "classical" and "new P_i" sites have been observed (as previously discussed) and that sometimes the P_i is less defined than the P_s site (*18*, *22*), it is difficult to deduce any functional relationship between catalytic activity and $SO_4$339 position.

In summary, by comparing the crystal structures of chloroplast GAPDH, complexed with either NAD (this paper) or NADP (*29*), and the crystal structure of *B. st.* GAPDH (*18*), as a well-analyzed example of glycolytic NAD-dependent GAPDH, it has been possible to single out the molecular determinants of coenzyme specificity in these dehydrogenases. The four residues Thr33, Ala40, Ala187, and Ser188 (Leu33, Leu40, Leu187, and Pro188 in most NAD-dependent GAPDHs) are all of primary importance for the dual cofactor specificity of photosynthetic GAPDH: Ala40, in particular, by allowing Asp32 (which interacts with NAD) to move away from the 2′-phosphate of NADP, and Thr33, Ala187, and Ser188 by directly providing room (Ala187) and interactions (Thr33, Ser188) for the allocation of the phosphorylated coenzyme. These modifications, therefore, seem to trace the minimal evolutionary route for a primitive NAD-specific GAPDH to be converted into the NAD(P)-GAPDH of oxygenic photosynthetic organisms.

ACKNOWLEDGMENT

We thank the Elettra Synchrotron Light Source (Trieste, Italy) for beam line access.

REFERENCES

1. Cerff, R. (1979) Quaternary structure of higher plant glyceraldehyde-3-phosphate dehydrogenases, *Eur. J. Biochem. 94*, 243−247.
2. Pupillo, P., and Faggiani, R. (1979) Subunit structure of three glyceraldehyde-3-phosphate dehydrogenases of some flowering plants, *Arch. Biochem. Biophys. 154*, 475−482.
3. Scagliarini, S., Trost, P., and Pupillo, P. (1998) The non-regulatory isoform of NADP(H)-glyceraldehyde-3-phosphate dehydrogenase from spinach chloroplasts, *J. Exp. Bot. 49*, 1307−1315.
4. Pupillo, P., and Giuliani Piccari, G. (1975) The reversibile depolymerization of spinach chloroplast glyceraldehyde-3-phosphate dehydrogenase. Interaction with nucleotides and dithiothreitol, *Eur. J. Biochem. 51*, 475−482.
5. Wolosiuk, R. A., and Buchanan, B. B. (1978) Studies on the regulation of chloroplast NADP-linked glyceraldehyde-3-phosphate dehydrogenase, *J. Biol. Chem. 251*, 6456−6461.
6. Wolosiuk, R. A., Hertig, C. M., and Busconi, L. L. (1986) Activation of spinach chloroplast NADP-linked glyceraldehyde-3-phosphate dehydrogenase by concerted hysteresis, *Arch. Biochem. Biophys. 246*, 1−8.
7. Trost, P., Scagliarini, S., Valenti, V., and Pupillo, P. (1993) Activation of spinach chloroplast glyceraldehyde-3-phosphate dehydrogenase: effect of glycerate 1,3-bisphosphate, *Planta 190*, 320−326.
8. Baalmann, E., Backhausen, J. E., Rak, C., Vetter, S., and Scheibe, R. (1995) Reductive modification and non-reductive activation of spinach chloroplast NADP-glyceraldehyde-3-phosphate dehydrogenase, *Arch. Biochem. Biophys. 324*, 201−208.
9. Sparla, F., Pupillo, P., and Trost, P. (2002) The C-terminal extension of glyceraldehyde-3-phosphate dehydrogenase subunit B acts as an autoinhibitory domain regulated by thioredoxins and nicotinamide adenine dinucleotide, *J. Biol. Chem. 277*, 44946−44952.
10. Harris, J. I., and Waters, M. (1976) Glyceraldehyde-3-phosphate dehydrogenase, in *The Enzymes* (Boyer, P. D., Ed.) Vol. 13, pp 1−49, Academic Press, New York.
11. Mayer-Gauen, M., Schnarrenberger, C., Cerff, R., and Martin, W. (1994) Molecular characterization of a novel, nuclear-encoded, NAD^+-dependent glyceraldehyde-3-phosphate dehydrogenase in plastids of the gymnosperm, *Pinus sylvestris L.*, *Plant Mol. Biol. 26*, 1155−1166.
12. Cerff, R. (1978) Glyceraldehyde-3-phospahte dehydrogenase from *Sinapis alba*: steady-state kinetics, *Phytochem. 17*, 2061−2067.
13. Koksharova, O., Schubert, M., Shestakov, S., and Cerff, R. (1998) Genetic and biochemical evidence for distinct key functions of two highly divergent GAPDH genes in catabolic and anabolic carbon flow of the cyanobacterium *Synechocystis* sp. PCC 6803, *Plant Mol. Biol. 36*, 183−194.
14. Figge, R. M., Schubert, M., Brinkmann, H., and Cerff, R. (1999) Glyceraldehyde-3-phosphate dehydrogenase gene diversity in eubacteria and eukaryotes: evidence for intra- and inter-kingdom gene transfer, *Mol. Biol. Evol. 16*, 429−440.
15. Buehner, M., Ford, G. C., Moras, D., Olsen, K. W., and Rossmann, M. G. (1974) Three-dimensional structure of D-glyceraldehyde-3-phosphate dehydrogenase, *J. Mol. Biol. 90*, 25−49.

16. Mercer, W. D., Winn, S. I., and Watson, H. C. (1976) Twinning in crystals of human skeletal muscle D-glyceraldehyde-3-phosphate dehydrogenase, *J. Mol. Biol. 104*, 277−283.
17. Griffith, J. B., Lee, B., Murdock, A. L., and Amelunxen, R. E. (1983) Molecular symmetry of glyceraldehyde-3-phosphate dehydrogenase from *Bacillus coagulans*, *J. Mol. Biol. 169*, 963−974.
18. Skarzynski, T., Moody, P. C. E., and Wonacott, A. J. (1987) Structure of the holo-glyceraldehydde-3-phosphate dehydrogenase from *Bacillus stearothermophilus* at 1.8 Å of resolution, *J. Mol. Biol. 193*, 171−187.
19. Vellieux, F. M. D., Hajdu, J., and Hol, W. G. J. (1995) Refined 3.2 Å resolution structure of glycosomal glyceraldehyde-3-phospate dehydrogenase from *Trypanosoma brucei brucei*, *Acta Crystallogr. D51*, 575−589.
20. Kim, H., Feil, I. K., Verlinde, C. L. M. J., Petra, P. H., and Hol, W. G. J. (1995) Crystal structure of glycosomal glyceraldehyde-3-phosphate dehydrogenase from *Leishmania mexicana*: implications for structure-based drug design and a new position for the inorganic phosphate binding site, *Biochemistry 34*, 14975−14986.
21. Korndörfer, I., Steipe, B., Huber, R., Tomschy, A., and Jaenicke, R. (1995) The crystal structure of holo-glyceraldehyde-3-phosphate dehydrogenase from hyperthermophilic bacterium *Thermotoga maritima* at 2.5 Å of resolution, *J. Mol. Biol. 246*, 511−521.
22. Duée, E., Olivier-Deyris, L., Fanchon, E., Corbier, C., Branlant, G., and Dideberg, O. (1996) Comparison of the structures of wild-type and a N313T mutant of *Escherichia coli* glyceraldehyde-3-phosphate dehydrogenases: implication for NAD binding and cooperativity, *J. Mol. Biol. 257*, 814−838.
23. Tanner, J. J., Hecht, R. M., and Krause, K. L. (1996) Determinants of enzyme thermostability observed in the molecular structure of *Thermus aquaticus* D-glyceraldehyde-3-phosphate dehydrogenase at 2.5 Å resolution, *Biochemistry 35*, 2597−2609.
24. Song, S., Li, J., and Lin, Z. (1998) Structure of the holo-glyceraldehyde-3-phosphate dehydrogenase from *Palinurus versicolor* refined at 2.0 Å of resolution, *Acta Crystallogr. D54*, 558−569.
25. Souza, D. H. F., Garratt, R. C., Araujo, A. P. U., Guimaraes, B. G., Jesus, W. P. D., Michels, P. A. M., Hannaert, V., and Oliva, G. (1998) *Trypanosoma cruzi* glycosomal glyceraldehyde-3-phosphate dehydrogenase: structure, catalytic mechanism, and targeted inhibitor design, *FEBS Lett. 424*, 131−135.
26. Isupov, M. N., Fleming, T. M., Dalby, A. R., Crowhurst, G. S., Bourne, P. C., and Littlechild, J. A. (1999) Crystal structure of the glyceraldehyde-3-phosphate dehydrogenase from hyperthermophilic archeon *Sulfolobus solfataricus*, *J. Mol. Biol. 291*, 651−660.
27. Charron, C., Talfournier, F., Isupov, M. N., Littlechild, J. A., Branlant, G., Vitoux, B., and Aubry, A. (2000) The crystal structure of D-glyceraldehyde-3-phosphate dehydrogenase from the hyperthermophilic archeon *Methanothermus fervidus* in the presence of $NADP^+$ at 2.1 Å of resolution, *J. Mol. Biol. 297*, 481−500.
28. Carugo, O., and Argos, P. (1997) NADP-dependent enzymes. I: Conserved stereochemistry of cofactor binding, *Proteins: Struct. Funct. Genet. 28*, 10−28.
29. Fermani, S., Ripamonti, A., Sabatino, P., Zanotti, G., Scagliarini, S., Sparla, F., Trost, P., and Pupillo, P. (2001) Crystal structure of the non-regulatory A_4 isoform of spinach chloroplast glyceraldehyde-3-phosphate dehydrogenase complexed with NADP, *J. Mol. Biol. 314*, 527−542.
30. Ferri, G., Stoppini, M., Meloni, M., Zapponi, M. C., and Iadarola, P. (1990) Chloroplast glyceraldehyde-3-phosphate dehydrogenase (NADP): amino acid sequence of the subunits from isoenzyme I and structural relationship with isoenzyme II, *Biochim. Biophys. Acta 1041*, 36−42.
31. Bergmeyer, H. U. (1985) *Methods of Enzymatic Analysis*, Verlag Chemie, Weinheim, Germany.
32. Segel, I. H. (1975) *Enzyme Kinetics*, John Wiley and Sons, New York.
33. Otwinowsky, Z., and Minor, W. (1993) Processing of X-ray diffraction data collected in oscillation mode, *Methods Enzymol. 276*, 307−326.
34. Sabatino, P., Fermani, S., Ripamonti, A., Cassetta, A., Scagliarini, S., and Trost, P. (1999) Crystallization and preliminary X-ray study of chloroplast glyceraldehyde-3-phosphate dehydrogenase, *Acta Crystallogr. D55*, 566−567.
35. Collaborative computational project n°. 4 (1994) The CCP4 suite: programs for protein crystallography, *Acta Crystallogr. D50*, 760−763.
36. Brünger, A. T., Adams, P. D., Clore, G. M., DeLano, W. L., Gros, P., Grosse-Kunstleve, R. W., Jiang, J. S., Kuszewski, J., Nilges, N., Pannu, N. S., Read, R. J., Rice, L. M., Simonson, T., and Warren, G. L. (1998) Crystallography and NMR system (CNS): A new software system for macromolecular structure determination, *Acta Crystallogr. D54*, 905−921.
37. Jones, T. A., Zou, J. Y., Cowan, S. W., and Kjeldgaard, M. (1991) Improved methods for building models in electron density maps and the location of errors in these models, *Acta Crystallogr. A47*, 110−119.
38. Bieseker, G., Harris, J. I., Thierry, J. C., Walker, J. E., and Wonacott, A. J. (1977) Sequence and structure of D-glyceraldehyde-3-phosphate dehydrogenase from *Bacillus stearothermophilus*, *Nature 266*, 328−333.
39. Moras, D., Olsen, K. W., Sabesan, M. N., Buehner, M., Ford, G. C., and Rossmann, M. G. (1975) Studies of asymmetry in the three-dimensional structure of lobster D-glyceraldehyde-3-phosphate dehydrogenase, *J. Biol. Chem. 250*, 9137−9162.
40. Corbier, C., Michels, S., Wonacott, A. J., and Branlant, G. (1994) Characterization of the two anion-recognition sites of glyceraldehyde-3-phosphate dehydrogenase from *Bacillus stearothermophilus* by site-directed mutagenesis and chemical modification, *Biochemistry 33*, 3260−3265.
41. Laskowski, R. A., MacArthur, M. W., Moss, D. S., and Thornton, J. M. (1993) PROCHECK: a program to check the stereochemical quality of protein structures, *J. Appl. Crystallogr. 26*, 283−291.
42. Luzzati, V. (1952) Traitement statistique des erreurs dans la détermination des structures cristallines, *Acta Crystallogr. 5*, 802−810.
43. Song, S. Y., Xu, Y. B., Lin, Z. J., and Tsou, C. I. (1999) Structure of active site carboxymethylated D-glyceraldehyde-3-phosphate dehydrogenase from *Palinurus versicolor*, *J. Mol. Biol. 287*, 719−725.
44. Yun, M., Park, C. G., Kim, J. Y., and Park, H. W. (2000) Structural analysis of glyceraldehyde-3-phosphate dehydrogenase from *Escherichia coli*: direct evidence of substrate binding and cofactor-induced conformational changes, *Biochemistry 39*, 10702−10710.
45. Correll, C. C., Ludwig, M. L., Bruns, C. N., and Karplus, P. A. (1993) Structural prototypes for an extended family of flavoprotein reductases: comparison of phthalate dioxygenase with ferredoxin reductase and ferredoxin, *Protein Sci. 2*, 2112−2133.
46. Heineke, D., Riens, B., Grosse, H., Hoferichter, P., and Heldt, H. W. (1991) Redox transfer across the inner chloroplast envelope membrane, *Plant Physiol. 95*, 1131−1137.
47. Fillinger, S., Boschi-Muller, S., Azza, S., Dervyn, E., Branlant, G., and Aymerich, S. (2000) Two glyceraldehyde-3-phosphate dehydrogenases with opposite physiological roles in a nonphotosynthetic bacterium, *J. Biol. Chem. 275*, 14031−14037.
48. Verho, R., Richard, P., Jonson, P. H., Sundqvist, L., Londesborough, J., and Penttilä, M. (2002) Identification of the first fungal NADP-GAPDH from *Kluyveromyces lactis*, *Biochemistry 41*, 13833−13838.
49. Clermont, S., Corbier, C., Mely, Y., Gerard, D., Wonacott, A., and Branlant, G. (1993) Determinants of coenzyme specificity in glyceraldehyde-3-phosphate dehydrogenase: role of the acidic residue in the fingerprint region of the nucleotide binding fold, *Biochemistry 32*, 10178−10184.
50. Reddy, S. G., Scapin, G., and Blanchard, J. S. (1996) Interaction of pyridine nucleotide substrates with *Escherichia coli* dihydropicolinate reductase: thermodynamic and structural analysis of binary complexes, *Biochemistry 35*, 13294−13302.
51. Kraulis, P. J. (1991) MOLSCRIPT: a program to produce both detailed and schematic plots of protein structures, *J. Appl. Crystallogr. 24*, 946−950.

BI0272149